GIScience & Remote Sensing

ISSN: 1548-1603 (Print) 1943-7226 (Online) Journal homepage: www.tandfonline.com/journals/tgrs20

Can we quantify the relationship between multispectral remote sensing images and land use and land cover maps? An explicit information transfer model based on Boltzmann entropy

Xinghua Cheng & Zhilin Li

To cite this article: Xinghua Cheng & Zhilin Li (2025) Can we quantify the relationship between multispectral remote sensing images and land use and land cover maps? An explicit information transfer model based on Boltzmann entropy, GIScience & Remote Sensing, 62:1, 2478689, DOI: 10.1080/15481603.2025.2478689

To link to this article: https://doi.org/10.1080/15481603.2025.2478689

© 2025 The Author(s). Published by Informa UK Limited, trading as Taylor & Francis Group.

Published online: 17 Mar 2025.

Submit your article to this journal

Article views: 1005

View related articles

View Crossmark data

Full Terms & Conditions of access and use can be found at
https://www.tandfonline.com/action/journalInformation?journalCode=tgrs20

GISCIENCE & REMOTE SENSING
2025, VOL. 62, NO. 1, 2478689
https://doi.org/10.1080/15481603.2025.2478689

Taylor & Francis
Taylor & Francis Group

OPEN ACCESS Check for updates

Can we quantify the relationship between multispectral remote sensing images and land use and land cover maps? An explicit information transfer model based on Boltzmann entropy

Xinghua Cheng [a,b] and Zhilin Li [a,b,c]

[a]Faculty of Geosciences and Engineering, Southwest Jiaotong University, Chengdu, China; [b]Department of Land Surveying and Geo-Informatics, The Hong Kong Polytechnic University, Hong Kong, China; [c]Shenzhen Research Institute, Southwest Jiaotong University, Shenzhen, China

ABSTRACT

Multispectral remote sensing images (MRSI) contain rich information about geographical objects and phenomena, such as land use and land cover. To extract such information, classification is normally carried out to yield land use and land cover maps (LULCM). A lot of techniques have been developed for classification, yet such a fundamental problem has not been solved as mathematical models for predicting the upper and lower limits of land cover classification accuracy with a given MRSI. This study aims to tackle this key problem by considering classification as an explicit information transfer process from images to maps and then build a mathematical model (Boltzmann-entropy-based) for the process with Shannon's information theory and Crooks' Thermodynamic Fluctuation as theoretical foundation. The model is designed to predict both upper and lower limits of classification accuracy instead of a definite value and is expressed in terms of Boltzmann entropies of MRSI and LULCM, total number of classes, and two basic parameters defined by prior knowledge. Verification experiments are carried out with 1091 images and three well-established classifiers (support vector machine, random forests, and K-nearest neighbors). The results demonstrate that (i) the values of information in MRSI and LULCM are strongly correlated, and (ii) the Boltzmann-entropy-based model can predict both upper and lower limits of classification accuracy. This study provides a novel perspective for understanding land cover classification and opens the door for the establishment of new theories in remote sensing.

ARTICLE HISTORY
Received 3 September 2024
Accepted 8 March 2025

KEYWORDS
Multispectral remote sensing images; land use and land cover map; classification accuracy limits; classification mechanism; information transfer model; Boltzmann entropy

1. Introduction

Multispectral remote sensing images (MRSI) record spatial, temporal, and spectral information about geographical objects and phenomena at field to global scales. Classification with MRSI plays a crucial role in generating land use and land cover (LULC) maps (hereafter referred to as LULCM) that has served as an important means of information acquisition for various applications, including ecological monitoring (Mahdavi et al. 2018; Sheng et al. 2016), forest mapping (Gale et al. 2021; Zhu and Woodcock 2014), urban studies (Fauvel, Chanussot, and Atli Benediktsson 2006; Hong et al. 2023; Zhu et al. 2022), and agricultural monitoring (Weiss, Jacob, and Duveiller 2020). To obtain high-quality LULCM from remote sensing images, classification techniques and theories have been developed (Stehman and Foody 2019; Yu et al. 2017; Yuan et al. 2020; Q. Zhu et al. 2022). From a technical viewpoint, land cover classification from MRSI is to abstract given classes from the complex world. From a theoretical standpoint, the land cover classification process is to make information content transferred from MRSI to LULCM (Olofsson et al. 2014; Stehman and Foody 2019). This raises longstanding questions as below:

- What is the optimal number of land cover classes for a given MRSI under a specific classification scheme?
- What level of accuracy could be expected from classification with a given MRSI and specified number of classes?
- How can the classification accuracy for a given LULCM be determined when using imperfect samples or lacking ground-truth data?

To address these questions, the past five decades saw great efforts made in technique innovation (Chen et al. 2024; Lin et al. 2017; Romero, Gatta, and Camps-Valls

CONTACT Zhilin Li dean.ge@swjtu.edu.cn

© 2025 The Author(s). Published by Informa UK Limited, trading as Taylor & Francis Group.
This is an Open Access article distributed under the terms of the Creative Commons Attribution License (http://creativecommons.org/licenses/by/4.0/), which permits unrestricted use, distribution, and reproduction in any medium, provided the original work is properly cited. The terms on which this article has been published allow the posting of the Accepted Manuscript in a repository by the author(s) or with their consent.

2016) and map accuracy assessment (Foody 2010; Gong, Wang, and Huang 2024; Stehman et al. 2022; Wickham et al. 2021, 2023; Wulder et al. 2006; Xing and Stehman 2024). Land cover classification is a complex process influenced by various factors, including landscape complexity, class distinctions, training sample size, sample quality, and the choice of classifiers (Heydari and Mountrakis 2018; Olofsson et al. 2014).

The methods for quantifying map accuracy fall into three categories: design-based approaches, such as the error matrix (Stehman 2009a; Wulder et al. 2006); Bayesian inference (Denham, Mengersen, and Witte 2009; Magnussen 2009); and model-based approaches (Khatami, Mountrakis, and Stehman 2017; Stehman 2009b). These methods significantly enhance our understanding of classification mechanisms. Recently, building on machine learning theory for multi-class classification, Gong, Wang, and Huang (2024) quantitatively described the relationship between classification accuracy and sample complexity. This suggests that the relationships among these factors in land cover classification can be quantitatively modeled. Such a model or theory can indeed provide cost-effective guidelines for predicting accuracy in unsampled regions, assessing and comparing thematic map quality, identifying errors, and refining maps prior to detailed evaluations (Heydari and Mountrakis 2018; Lu and Weng 2007; Stehman and Foody 2019). However, developing such a mathematical model remains challenging due to several issues, as outlined below:

- The first challenge is to understand the land cover classification process in a logistically feasible way, utilizing appropriate statistical methods (Stehman and Foody 2019).
- The second challenge is to develop a metric that quantifies the spatial and spectral information within and between MRSI and LULCM (Foody and Mathur 2006) and to establish connections between these metric and reliable mathematical principles or laws.
- The third challenge is to model the relationship between local and global information in MRSI and LULCM, as high-quality land cover classification requires both strong local consistency and meaningful global diversity (Ma et al. 2023; Zhu et al. 2022).

To address these challenges, we apply concepts and theories from statistical thermodynamics and information theory to develop a novel model for land cover classification. The remainder of this article is organized as follows: Section 2 outlines the conceptual framework for understanding the land cover classification mechanism. Upon this foundation, Section 3 builds a mathematical model for information transfer and introduces a variation index. Section 4 details the verification experiments and analyzes the results. Finally, Sections 5 and 6 conclude the article with a discussion and final remarks.

2. Modeling information transfer in land cover classification: basic ideas

This section describes three key facets of land cover classification. We theoretically describe the information transfer from MRSI to LULCM through the concept of data compression, characterize the variation in land cover classification, and quantify this variation using the concepts of "*fluctuation*" and Boltzmann entropy from statistical thermodynamics.

2.1. The nature of land cover classification: data compression

Land cover classification involves categorizing spatially and categorically continuous objects and phenomena into discrete classes, which are then reorganized into a map format. This process can be viewed as a form of data compression, as the volume of data is effectively reduced. Letting MRSI as the variable X, the average coding length for X, denoted as $L(X)$, is defined as

$$L(X) = \sum_{x \in X} p(x) l(x) \tag{1}$$

where l(x) and p(x) are the code length of x and the probability mass function, respectively. Shannon et al. (1948) claimed that the minimum coding length $L(X)$ in lossless compression is bounded by $[H(X), H(X)+1]$, where $H(X)$ is the Shannon entropy of X, measured in bits. In principle, if the original data can be fully restored without any loss, the process is termed lossless compression; otherwise, it is called lossy compression. Similarly, in land cover classification, the ideal scenario involves accurately assigning a label to each pixel, highlighting the presence of both upper and lower limits.

2.2. Land cover classification: information transfer

Land cover classification from MRSI is an irreversible process of information transfer, as shown in Figure 1. Features are usually extracted from an MRSI and mapped into different spaces according to an objective function, resulting in a trained classifier. The classifier is then employed to convert the MRSI into an LULCM. During the classification process, pixels in different regions of the image may be assigned the same label (e.g. waterbody). However, there is no guarantee that each pixel is correctly classified, as illustrated in Figure 1(b), where pixels that should be labeled as "tree" are mistakenly assigned other labels. Figure 1(d-f) shows how variations in extracted features and their divisions result in different LULCMs. This outcome can be attributed to differences in the distribution of pixels of interest, their surrounding objects, and the representation of features extracted from the MRSI.

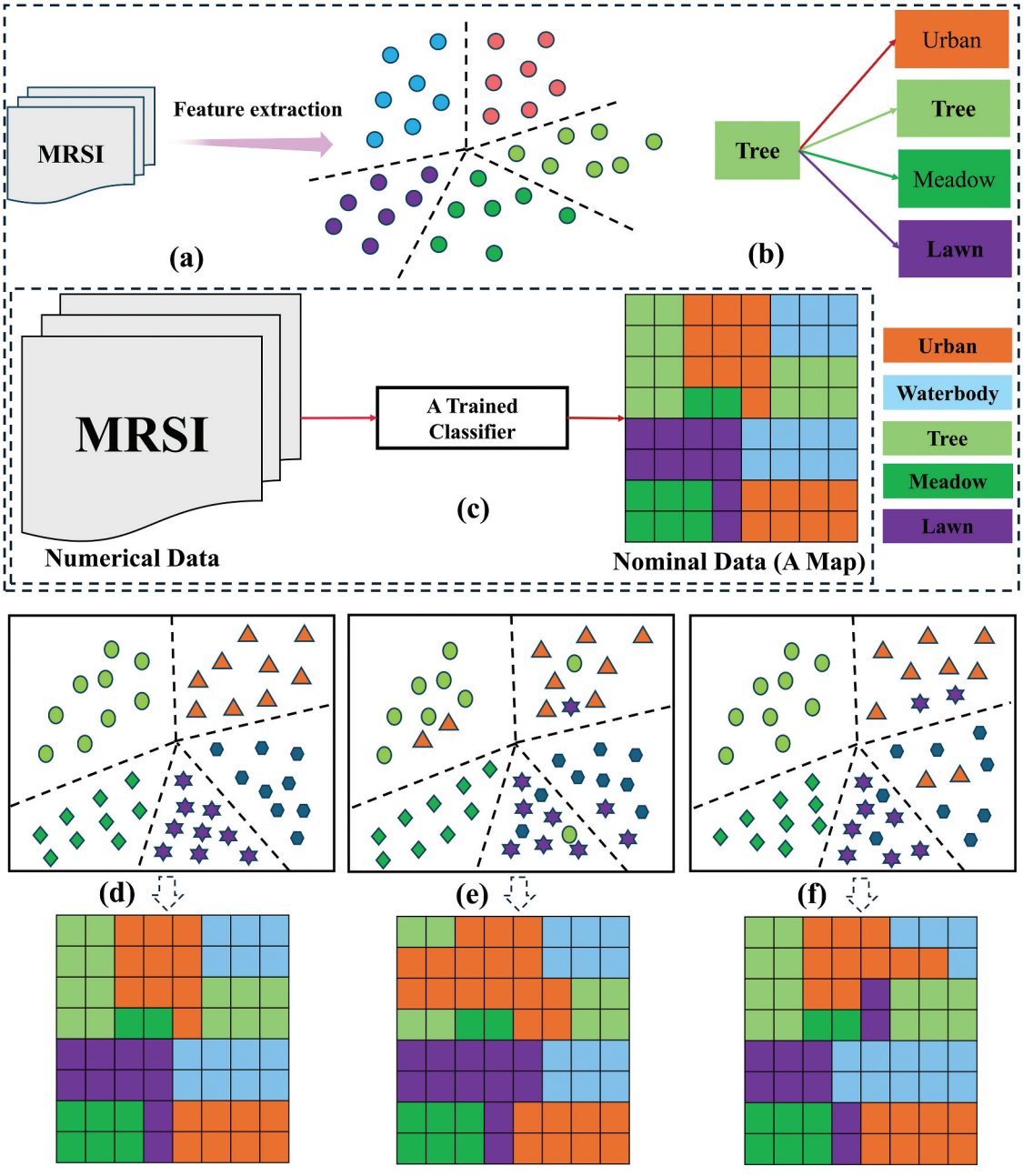

Figure 1. A technical flowchart of land cover classification. Top: (a) Feature extraction from MRSI for classifier training; (b) A pixel belonging to a 'tree' is incorrectly labeled; (c) Land cover classification alters the data (information) format. Bottom: divergent maps resulting from classifiers trained on distinct feature distributions.

The land cover classification process above indicates the variation in the MRSI-LULCM relationship (Heydari and Mountrakis 2018; Lu and Weng 2007; Stehman and Foody 2019). Characterizing such variations requires quantifying the intricated internal and external relationships of geographical objects at local to global scales. This includes, for example, the distribution of pixels within the same semantic object and their co-occurrence (Q. Zhu et al. 2022). While Shannon's information theory provides valuable insights, it is limited in directly quantifying the spatial structures within MRSI and LULCM (Cheng and Li 2021, 2023; Gao, Li, and Zhang 2018). To address this, we define a semantic object of interest as a macrostate (a system description from a macroscopic perspective, e.g. impervious surface) and consider the individual pixels comprising the object throughout the image as microstates (a more detailed description of the macrostate, such as buildings and concrete roads). With this definition, we can explore the mechanism linking MRSI to LUCLM through classification, accounting for both the upper and lower limits.

2.3. Land cover classification: local and global variations

Building on the theoretical description of land cover classification in Sections 2.1 and 2.2, this section introduces the quantification unit for constructing the mathematical model, which is determined by two key factors: local consistency and global diversity (Stehman and Wickham 2011; Zhu et al. 2022). We select a 2×2 patch as the minimum spatial unit because of (i) effectiveness in quantifying information content (Gao, Zhang, and Li 2017; Stehman and Wickham 2011) and (ii) simplicity and flexibility in determining agreement between MRSI and LULCM.

Figure 2 (a)-(f) illustrates six examples of converting six 2×2 MRSI patches into LULCM. The structure of each 2×2 patch directly influences local spatial variation, which in turn contributes to the overall structural diversity of the entire LULCM, as shown in Figure 2(g-i). In theory, the more complex an MRSI patch, the greater the heterogeneity of its corresponding LULCM.

For the 2×2 patch, an information metric is needed. This metric should enable users to (i) consistently quantify information content of MRSI and LULCM, (ii) explicitly build a link between information transfer and well-established laws, and (iii) directly analyze the information transfer across multiple spatial scales. This study selects Boltzmann entropy as such a measure.

2.4. Boltzmann entropy as a proxy for quantifying information transfer

Boltzmann entropy (Boltzmann 1872), also known as thermodynamic entropy, is a fundamental metric in statistical thermodynamics that links phenomena at the microstate level to those at the macrostate level. It is defined as follows:

$$S = k_b \log W \tag{2}$$

where W is the number of possible microstates for a given macrostate and k_b is the Boltzmann constant.

Gao, Zhang, and Li (2017) made use of the ideas of integration in calculus to calculate the Boltzmann entropy of any data organized in raster format. They partitioned the entire image into a series of 2×2 patches, defining the aggregated result of the pixels within each 2×2 patch as the macrostate, with all the possible permutations that downscale the macrostate to the original resolution considered as microstates. Such a "from-to" way is grounded in the principle of hierarchical representation. Here, the information content of MRSI is quantified using Boltzmann entropy, denoted as S_{MRSI}, and is expressed through

$$S_{MRSI} = \sum_{m \in M} \log W_m \tag{3}$$

where M denotes a patch ensemble comprising a MRSI, m represents a 2×2 patch, and W_m is the total number of microstates. The calculation of S_{MRSI} is implemented using a 2×2 moving window across the entire MRSI, allowing Equation (3) to be rewritten as

$$S_{MRSI} = \prod_{r=1}^{R} \prod_{c=1}^{C} \log W_{r,c} \tag{4}$$

where R and C are the rows and columns, respectively, $W_{r,c}$ is the number of microstates of the patch located in r^{th} row and c^{th} column.

Similarly, Boltzmann entropy of a LULCM, S_{LULCM}, is defined as:

$$S_{LULCM} = \sum_{n \in N} \log W_n \tag{5}$$

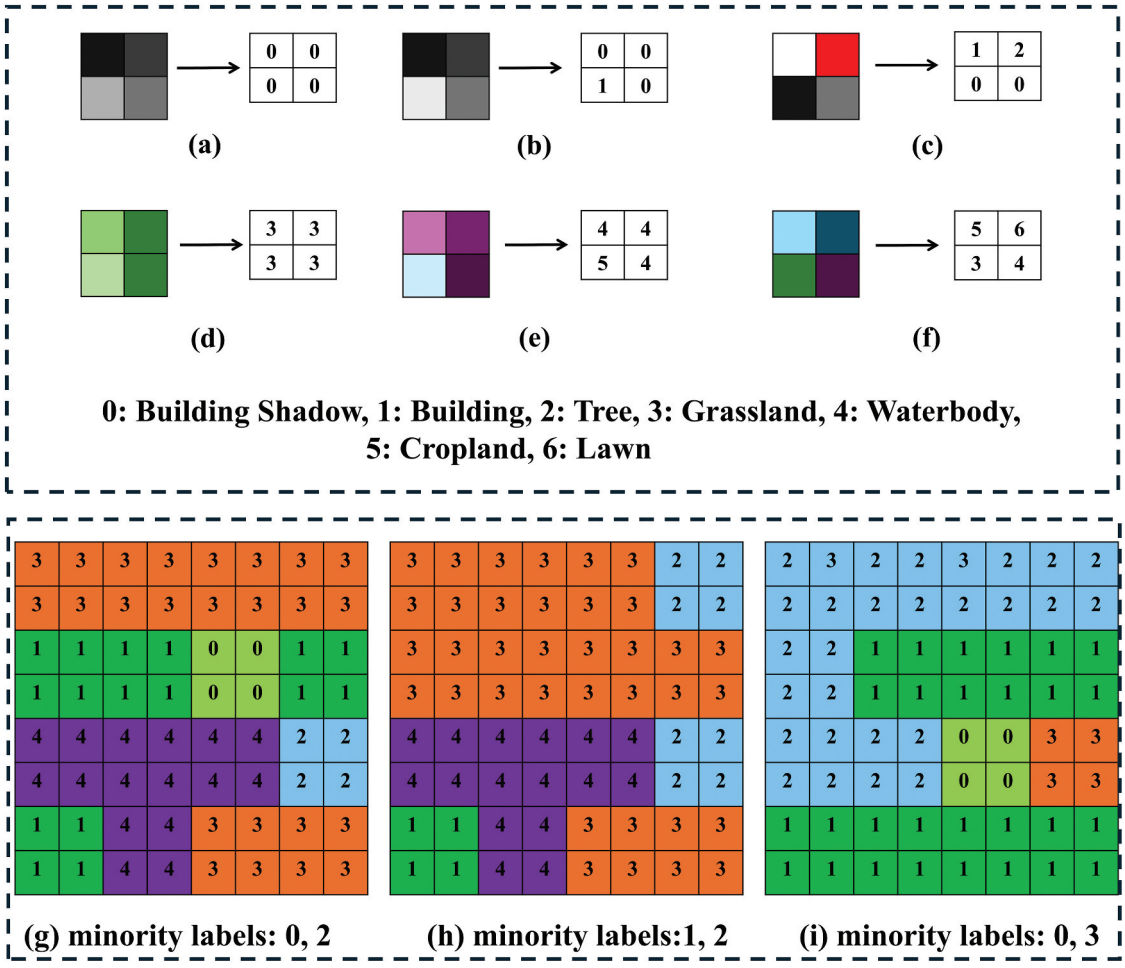

Figure 2. Information transfer at local to global scales. Top: information transfer at a 2×2 patch, where the colors of circles represent numerical values. Bottom: structure of the LULCM, showing the effects of imbalanced land cover classes and spatial variation of local patches.

where W_n is the number of all possible permutations (i.e. the total number of classes and their percentages) for a 2×2 window (Gao and Li 2019), N is the total number of 2×2 windows.

The alignment of the definitions of Boltzmann entropy for MRSI and LULCM ensures consistency, offering us reliable tools to model the information transfer. This study uses a logarithmic base of 2 and applies the resampling-based approach (Gao, Zhang, and Li 2017) instead of the aggregation-based method (Gao and Li 2019) to calculate S_{MRSI} and S_{LULCM}, with the unit of bits per pixel. This is because previous studies have shown that the resampling-based approach where the sliding computation windows are overlapped outperforms the aggregation-based method (Cheng and Li 2021; Cheng and Yeung Yan 2025; Gao et al. 2018). This study further defines the information content difference, ΔS, between two images or maps. Given that both S_{MRSI} and S_{LULCM} are inherently integral results at the scale of 2×2 patch, ΔS is defined as:

$$\Delta S = \frac{S_a - S_b}{S_b} \times 10^{d-1} \tag{6}$$

where d represents the number of digits in the image dimensions (e.g. $d = 3$ for an MRSI of size 512×512), a and b are either MRSI or LULCM of the same dimension (for different dimensions, readers can refer to Cheng and Li (2021)). As shown in Figure 3, the four MRSIs display identical compositions yet have different S_{MRSI} values. Similar variations are observed in the four LULCMs that exhibit distinct structure patterns. The ΔS between Figure 3(b) and (a) is 15.23 bits per pixel and that between (f) and (e) is 92.51 bits per pixel.

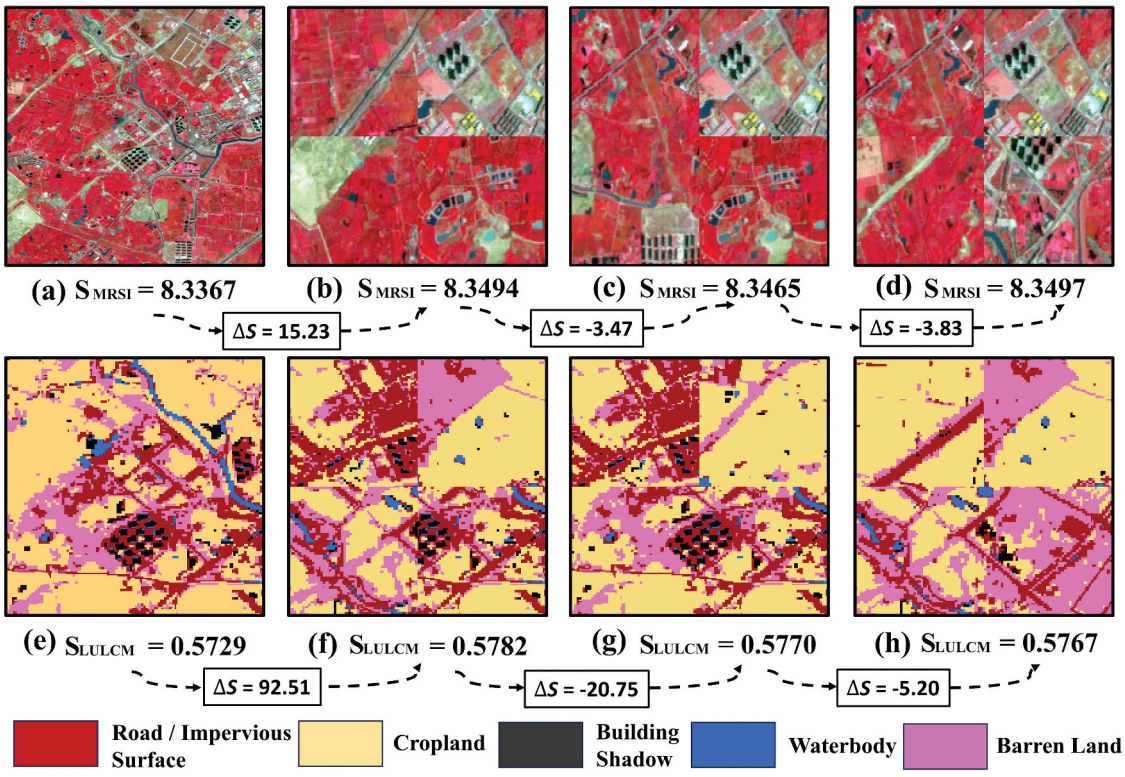

Figure 3. The structural information content of MRSI and LULCM quantified by Boltzmann entropy. The size of each image is 512 × 512. First row: four MRSIs displayed in a false color, where and (b)-(d) are scrambled versions of (a). Second row: four LULCMs, with (f)-(h) representing scrambled versions of (e).

3. Modeling information transfer with Boltzmann entropy

To develop a Boltzmann-entropy-based model, guidance from well-established laws is essential; therefore, we draw on concepts and principles from Crooks' Fluctuation Theorem (CFT, Crooks 1999).

3.1. Quantification of variation in thermodynamics: Crooks' Fluctuation Theorem

The second law of thermodynamics states that the entropy (degree of disorder) of an isolated and closed system will increase spontaneously until it reaches thermodynamic equilibrium, at which entropy is maximized. Figure 4 illustrates how the movement of gas molecules results in various states, where interactions between molecules influence movement directions. The complex interplay between molecular motion and interaction ultimately dictates the configuration.

Cooks' Fluctuation Theorem describes the "*fluctuation*" (hereafter referred to as variation) in Figure 4, which reads

$$\frac{P_F(EP)}{P_F(-EP)} = e^{\frac{S}{k_b}} \tag{7}$$

where $P_F(EP)$ and $P_F(-EP)$ represent the probability of entropy production along the forward and reverse path, respectively. EP is a measure for quantifying the process efficiency and is calculated as follows:

$$EP = \frac{W-\Delta F_{sys}}{T} \tag{8}$$

where W is the work acting on a closed system, ΔF_{sys} is the free energy difference between two states, and T is the temperature. Consequently, Equation (7) can be written as

$$\frac{P_F(EP)}{P_F(-EP)} = e^{\frac{W-\Delta F_{sys}}{Tk_b}} \tag{9}$$

where k_b represents the Boltzmann constant, and T retains the same meaning as in Equation (8).

Building on CFT, we assume that a trained classifier performs "work" on an MRSI to convert it into an LULCM based on specified land cover classes, resulting in a change in data type from numeric to nominal. This "work" determines the number of correctly classified

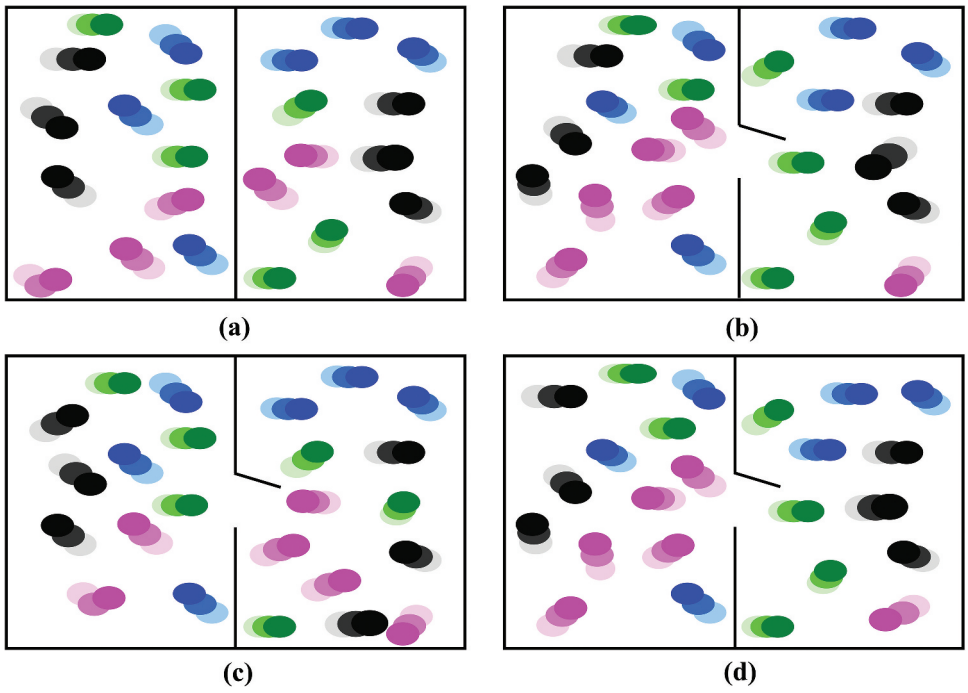

Figure 4. Example of gas molecule movement in a closed thermodynamic system. (a): the system in its initial state. (b)-(d): molecular movement leads to structural changes in the system, reflecting variations in entropy and changes in free energy (Crooks 1999).

pixels, thereby affecting the structural and classification accuracy across the entire region of interest.

3.2. An information transfer model with Boltzmann entropy

Recognizing the critical importance of distinguishing between mathematical and physical assumptions, this study selects the information content, quantified by Boltzmann entropy, as a proxy for the energy of MRSI and LULCM, with classification accuracy serving as a potential indicator of "work."

We consider an MRSI or map as an assemble $\Omega = \{imp_1, imp_2, imp_3, \cdots imp_n\}$, composed of 2×2 patches. The "work" applied to a 2×2 image patch, denoted as W_{imp}, is defined as:

$$W_{imp} = \eta_{imp} \times S_{imp} \tag{10}$$

where η_{imp} denotes the working efficiency of a trained classifier, represented as classification accuracy, and S_{imp} is the Boltzmann entropy. The total work applied to an MRSI is calculated as follows:

$$W = \iint \eta_{imp} \times S_{imp} d(S_{imp}) d(\eta_{imp}) \tag{11}$$

Solving Equation (11) is impossible in real-world applications, as assigning a ground-truth label to each pixel for calculating classification accuracy is unfeasible (Olofsson et al. 2014). Thus, according to the law of large number, we approximate W with

$$W = C \times S_{MRSI} \tag{12}$$

where C is the classification accuracy measure (e.g. F1-score), S_{MRSI} is the one in Equation (4).

Building on Equations (4) to (12), the MRSI-LULCM relationship (MLR) can be quantified, incorporating prior knowledge from (i) the logarithmic function employed in Shannon's information theory and (ii) the well-established premise that the number of land cover classes is theoretically infinite. The mathematical form of MLR is

$$\frac{S_{LULCM}}{N_c} = e^{\frac{\beta \times k_b \times C \times S_{MRSI}}{T} - g} \tag{13}$$

where both k_b and T are set to 1 (Cushman 2016), $\frac{S_{LULCM}}{N_c}$ denotes the analogy of entropy production, denoted as the information transferred from MRSI, N_c is the total number of land cover classes, β and g are two basic parameters. The parameter β is introduced to address the uncertainty in determining the actual values of k_b and classification accuracy in the unsampled region. The inclusion of parameter g accounts for a practical scenario where S_{LULCM} becomes exceedingly small, effectively approaching

zero, when the MSRI reaches a homogeneous state (Heydari and Mountrakis 2018). To account for imbalanced classes, we use $\frac{1}{N_c}$ to characterize information transfer at the pixel level.

The mathematical definition of MLR above aligns with the well-established rule that a completely homogeneous MRSI will be assigned only one label. For simplicity, we represent MLR as $f(S_{MRSI}, z_m, S_{LULCM})$, where z_m represents the average of information transfer, to describe the trend in S_{LULCM} as S_{MRSI} increases.

3.3. Variation in MRSI-LULCM relationship: upper and lower bounds

Building upon the theoretical MLR, this section further offers the definition of the upper (z_u) and lower bounds (z_l), shown in Figure 5. Theoretically, as an MRSI increases in spectral and structural complexity (i.e. with a higher S_{MRSI} value), the resulting LULCMs become more intricate, highlighting the widening gap between the upper and lower bounds.

Here, we define the variation of such a gap as follows:

$$\delta_u = \int |f(S_{MRSI}, z_u, S_{LULCM}) - f(S_{MRSI}, z_m, S_{LULCM})| dS_{MRSI} \quad (14)$$

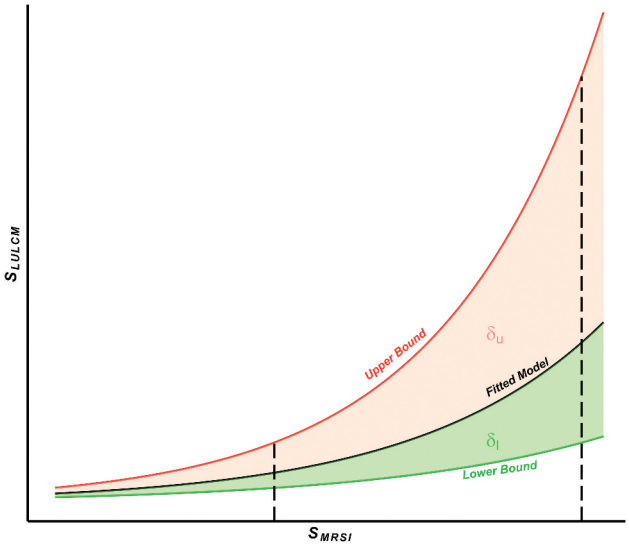

Figure 5. Diagram of defining the upper and lower bounds of MLR. The solid black curve represents the fitted model for MLR. The curves for the upper and lower bounds are constructed with the fitted model. δ_u is the area between the upper bound and the fitted model, while δ_l represents that between the fitted model and the lower bound.

$$\delta_l = \int |f(S_{MRSI}, z_m, S_{LULCM}) - f(S_{MRSI}, z_l, S_{LULCM})| dS_{MRSI} \quad (15)$$

where z_m, z_u, and z_l represent MLR, upper, and lower bounds, respectively, and δ_u and δ_l denote the variations for the upper and lower bounds, respectively.

Furthermore, an index for variation is defined as

$$GI_v = \frac{\delta_u}{\delta_l} \quad (16)$$

3.4. Determination of the threshold of S_{MRSI}

Determining an acceptable accuracy level is essential in land cover classification. For modeling information transfer, it is necessary to establish a threshold of S_{MRSI} (hereafter referred to as S_{thres}). Starting from a state of absolute homogeneity (i.e. $S_{MRSI} = 0$), an MRSI progressively increases in complexity, approaching absolute heterogeneity at which point S_{MRSI} is theoretically maximized. However, for specific land cover classes and a given trained classifier, S_{LULCM} will not always increase substantially. Drawing inspiration from the second law of thermodynamics, this study adopts 9.0 as the value for S_{thres}, that has been experimentally validated in previous studies (Cheng and Li 2021, 2023).

4. Experimental verification

4.1. Land cover classification experiment

To test the proposed model, we utilize cloud-free Sentinel-2 and Landsat 8 imagery from 2015 to 2022, as shown in Figure 6. The size of each experimental image is 512×512. Given the cloud-free requirement and selected areas, the dataset includes 279 Landsat images and 812 Sentinel-2 images. To obtain accurate parameters, 80% of these image samples are used to train the model, while the remaining 20% are reserved for validation.

We use three classical classifiers including Random Forest (RF, Breiman 2001), Support Vector Machine (SVM), and k-Nearest Neighbors (KNN, Franco-Lopez, Ek, and Bauer 2001) to implement land cover classification as they are well-established, stable, and computationally efficient. Classification experiments are conducted with Python 3.7 and scikit-learn (Pedregosa et al. 2011). To eliminate salt-and-pepper noise, we apply object-based post-classification refinement

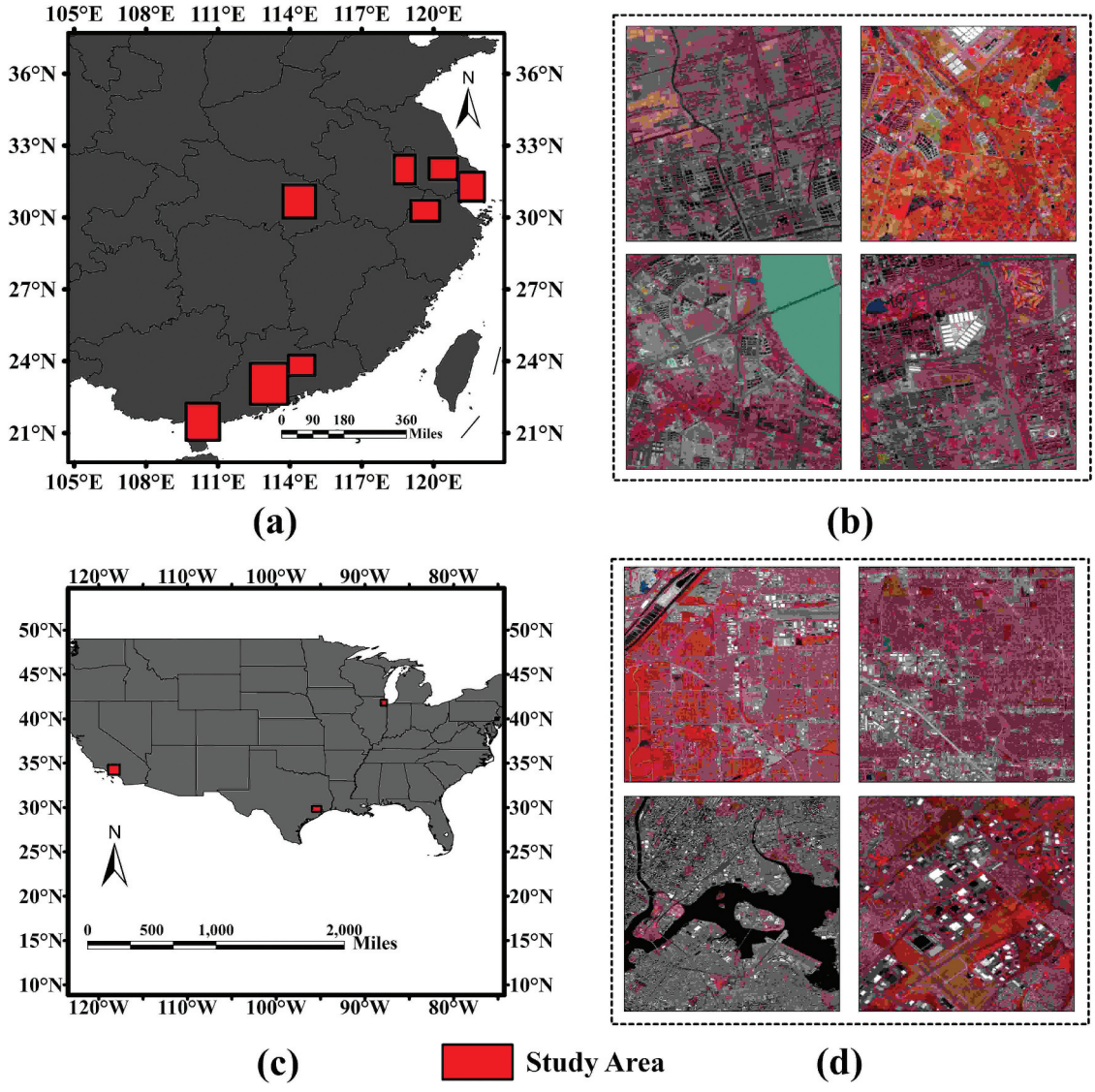

Figure 6. Overview of study areas and experimental images. (a) and (c) show the study areas in China and the contiguous US, respectively. (b) and (d) provide examples of eight experimental image examples covering urban and rural scenarios, illustrating both homogeneity and heterogeneity.

(OBPR) to improve the pixel-based classification results. Geographic objects are extracted from the images using the multi-resolution segmentation algorithm in eCognition 9.0.1 (Benz et al. 2004). The experimental images are categorized into nine classes: barren land, impervious surface/road, cropland, shrub, forest, waterbody, building shadow, grassland, and wetland. Class samples are collected randomly through visual interpretation of very high-resolution satellite images in ArcGIS Pro 3.0.3. Cases are excluded if the overall classification accuracy is below 85% (Anderson 1971) or if evident classification errors are observed upon visual interpretation.

Determining the upper and lower bounds relies on the fitted line for the land cover classification results. Therefore, in addition to the use of model in Equation (13), we employ PolyRatio (1,1) model, polynomial model, power model, and Michaelis Menten model for the fitting. The Akaike information criterion (AIC) is selected for determining which one is the best. Once the fitted model is selected, the upper and lower limits are thus determined and examined by

$$PA = \frac{N_{bounded}}{N_{all}} \times 100\% \quad (17)$$

where PA is prediction accuracy, N_{all} denotes the total number of test cases, $N_{bounded}$ is the number of cases included by the upper and lower bounds.

4.2. Variation in information transfer verified

As spatial and spectral complexities increase from (a) to (d), S_{LULCM} accordingly rises, as shown in Figure 7. It is evident that Boltzmann entropy captures the discernible trend. When the S_{MRSI} is larger than 9.0, however, the corresponding S_{LULCM} does not follow the trend of S_{MRSI}. This can be seen in land cover classification results for MRSIs (e) and (f).

MRSI (a) and (b) are visually more homogeneous than (c) and (d). Thus, for a given trainer classifier, S_{LULCM} of (a) and (b) are smaller than those of (c) and (d). However, the capabilities of RF, SVM, and KNN lead to S_{LULCM} differences. For (c), KNN yields the maximum S_{LULCM} (0.8147), while RF provides the minimum (0.7295). For (d), SVM yields the maximum S_{LULCM} (0.8353), whereas RF produces the minimum (0.7825). For (a) and (b), the variation in information transfer is reflected in S_{LULCM} difference: (i) SVM (0.4384) < RF (0.4401) <KNN (0.4782), (ii) RF (0.4775) < KNN (0.5146) < SVM (0.5460). Overall, the six cases demonstrate that the upper and lower bounds for S_{LULCM} exist, and Boltzmann entropy effectively captures the variation in information transfer from MRSI to LULCM.

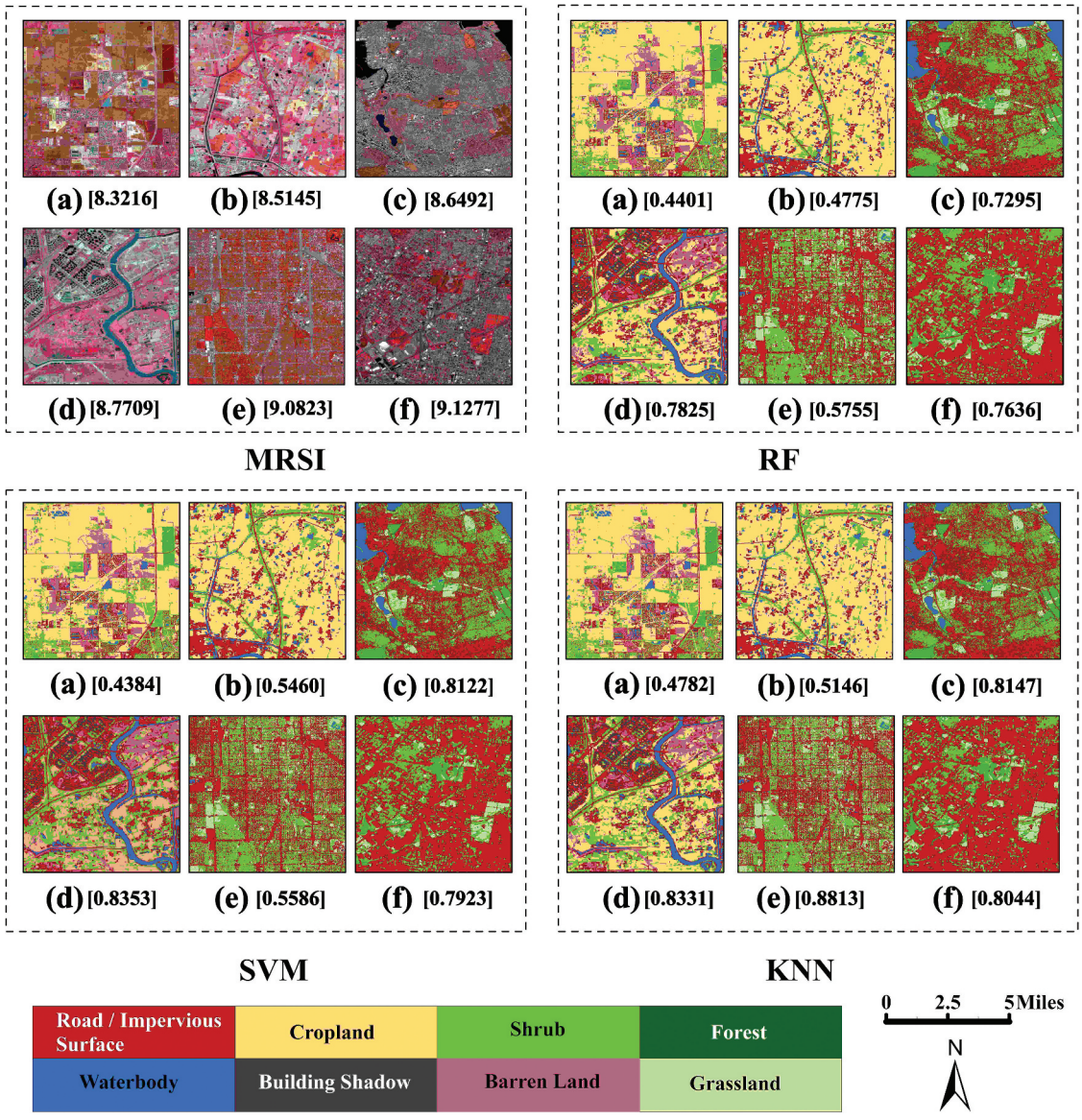

Figure 7. Land cover classification results for nine MRSIs. Boltzmann entropy values in bits per pixel are indicated in the square brackets.

4.3. Information transfer from MRSI to LULCM at patch to global scale

Figure 8 presents six MRSIs and their corresponding LULCMs at the patch scale. Figure 8(f) represents an urban scenario, characterized by high heterogeneity, while Figure 8(a) depicts an agricultural scenario, exhibiting significant homogeneity. Minimal visual differences are observed in the LULCM patches shown in Figure 8 (b) and (c). However, such structural differences at the patch scale directly contribute to the variations in S_{LULCM}.

We further examine the information transfer at the patch scale. Figure 9 presents classification results for six MRSIs, while Table 1 provides the differences in S_{LULCM} and S_{MRSI} among six patches. Notably, Boltzmann entropy of a patch can exceed that of the entire LULCM or MRSI.

In Figure 9(I), S_{MRSI} values of MRSI patches *b* (9.0082) and *f* (9.0284) exceed the S_{LULCM} calculated at the entire image scale, which is 8.9791 bits per pixel. In Figure 9(II), both MRSI patches *a* (S_{MRSI} = 9.0220) and *f* (S_{MRSI} = 9.1586) are more complex than other patches in the entire MRSI. Similar cases are observed in LULCMs. For the entire image, ΔS of MSRI between (II) to (I) and between (III) to (I) are 4.09 and 4.50, respectively. Accordingly, ΔS of corresponding LULCMs are 14.89 and 20.79, respectively. It is obvious that little ΔS difference in MSRI can result in substantial ΔS difference in LULCM.

4.4. Boltzmann-entropy-based model for upper and lower bounds of land cover classification

Figure 10 demonstrates the fitted models, upper and lower bounds. The upper panel graphically illustrates five fitted models, indicating the proposed Boltzmann-entropy-based model is the best one. The GI_v values are 2.05 for RF, 2.05 for SVM, and 1.74 for KNN. It is evident that the upper and lower bounds for results obtained with RF are superior to those from SVM and KNN. As S_{MRSI} increases, the gap between the upper bound and the fitted line accordingly widens.

Table 2 shows the mathematical formulas for the upper and lower bounds. This study recommends the one obtained with RF as follows:

$$S_{LULCM} = \begin{cases} e^{0.57\times S_{MRSI}-6.53} & upper\ bound \\ e^{0.86\times S_{MRSI}-9.80} & lower\ bound \end{cases}$$

where S_{MRSI} is ranged from (0, 9]. The case where S_{MRSI} equals to 0 represents an ideal scenario. The rationale for this recommendation is that the format and the parameters of the upper and lower bounds are closely aligned, and RF demonstrates superiority over both KNN and SVM.

The first and second derivatives of fitted model for RF-based cases are $0.63\times\ e^{0.57\times S_{MRSI}-6.53}$ and $0.3969\times\ e^{0.57\times S_{MRSI}-6.53}$, respectively. These two derivatives indicate that land cover classification results in compact information gain, provided that a high classification accuracy is achieved first.

Figure 11 visualizes the examination results of the recommended Boltzmann-entropy-based model, the prediction accuracy (PA) is very high (around 98%) for those $S_{MRSI} \leq S_{thres}$ (9.0). It is consistent with Section 3.4. To accurately predict those outside the bounds when S_{MRSI} value exceeds 9.0, model calibration is necessary to obtain the optimal parameters.

5. Discussion

Investigation of the information flow and transfer holds great potential for advancing reliable domain knowledge in land cover classification (Baraldi, Bruzzone, and Blonda 2005; Ebrahimy et al. 2021). In such a case, an index is particularly desirable because researchers usually use indices (e.g. normalized difference vegetation index) to encapsulate domain knowledge (Li et al. 2022; Ma et al. 2023) and subsequently design corresponding loss functions. In contrast, this study developed information-flow-based models to explicitly quantify the land cover classification process.

For future research, two directions can be explored. The first direction focuses on modeling information transfer across multiple spatial and spectral scales. Based on high-resolution multispectral images and advanced classifiers, it is promising to achieve both high classification accuracies and high-resolution land use and land cover maps. Deep learning techniques (e.g. convolution neural networks) have outperformed traditional classifiers through capturing multi-scale information (Hong et al. 2023; Tong et al. 2020). When using such techniques for land cover classification, we need to first determine the spatial and spectral scales at which the extracted information from images is

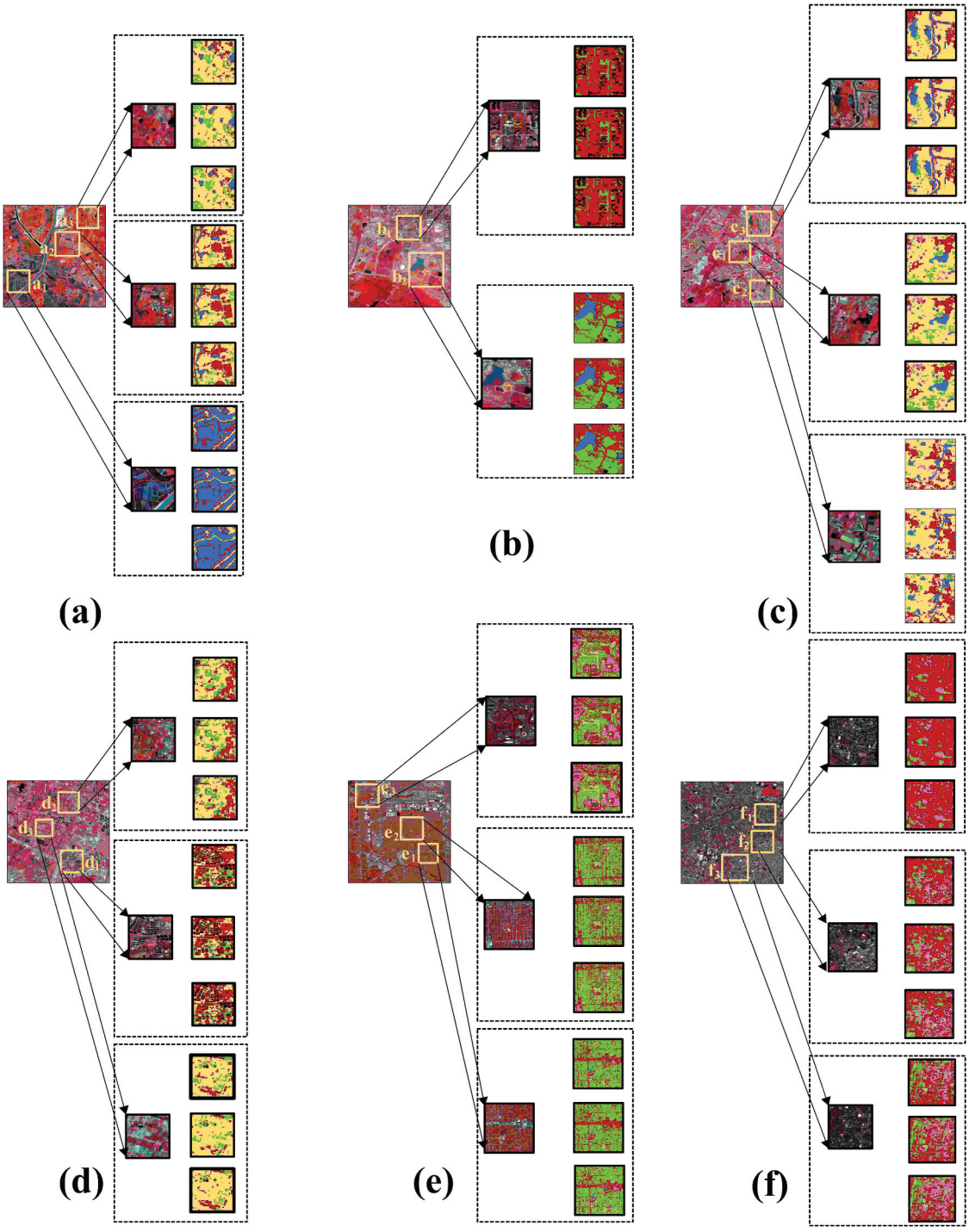

Figure 8. Visualization of land cover classification results at patch scale. The zoomed parts show the LULCM difference of patches across three classifiers: top (RF), middle (SVM), and bottom (KNN).

maximum. To further quantify the information transfer, a potential approach is to integrate absolute Boltzmann entropy (Gao, Zhang, and Li 2017, 2019) with Shannon entropy for quantifying information flow across all stages of land cover classification.

he second direction is modeling the spatial-temporal information transfer in land cover classification when utilizing multi-source remotely sensed images. In principle, integrating multiple spatial and temporal features from various data sources (e.g. Landsat, Sentinel-2, and MODIS) on

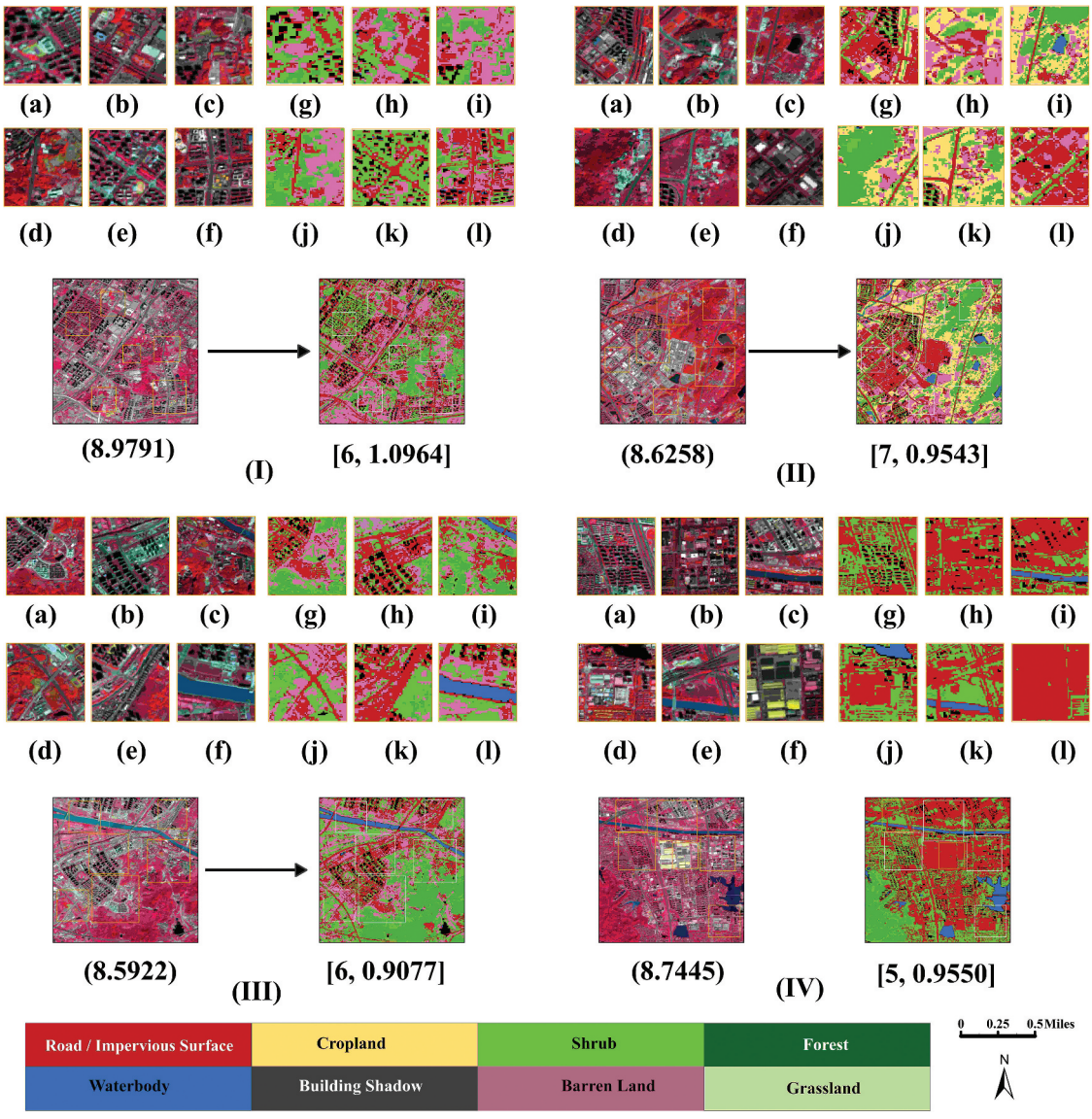

Figure 9. Four cases of information transfer at local to global scales. Cases (I) to (II) include both homogeneous patches (e.g. forest) and heterogeneous patches (e.g. impervious surface). Digits in parentheses denote S_{MRSI} value in bits per pixel. In the square bracket, the first digit represents the total number of classes in the entire LULCM, and the second digit indicates S_{LULCM} value in bits per pixel.

Table 1. Boltzmann entropy of MRSIs. The first item in square brackets indicates the total number of classes, and the second represents the Boltzmann entropy value in bits per pixel. Bold represents the maximum one.

Area	*a*	*g*	*b*	*h*	*c*	*i*	*d*	*j*	*e*	*k*	*f*	*l*
I	8.8920	[6,1.2081]	**9.0082**	[6, 1.0759]	8.8378	[6, 0.9312]	8.6240	[5, 0.9419]	**8.9645**	[6, **1.1721**]	9.0284	[6, **1.2329**]
II	**9.0220**	[7,1.1545]	8.4881	[6, 0.9610]	8.2768	[7, 0.8445]	8.0148	[7, 0.6689]	8.4540	[7, 0.9681]	**9.1586**	[6, 1.0837]
III	8.7455	[6,1.0373]	8.9460	[6, **1.1533**]	8.6051	[6, **1.0001**]	8.6404	[5, 0.9003]	8.7796	[6, 1.1290]	8.4407	[6, 0.8457]
IV	8.8712	[4,**1.2503**]	9.0471	[4, 0.9918]	8.7980	[5, 0.9323]	**8.7209**	[5, **0.9971**]	8.5488	[5, 1.0155]	9.0822	[2, 0.4465]

the same area can improve land cover classification (Chen, Huang, and Xu 2017; Hartling, Sagan, and Maimaitijiang 2021; Zhu and Woodcock 2014). In this case, we first need to quantify the amount of information that can be extracted, determine how much information can be ingested into the classifier, and quantify information loss before obtaining land use and land cover maps. Importantly, to better explicitly interpret multi-resource remote sensing data-based land cover classification, a better form of information flow and an end-to-end framework are needed.

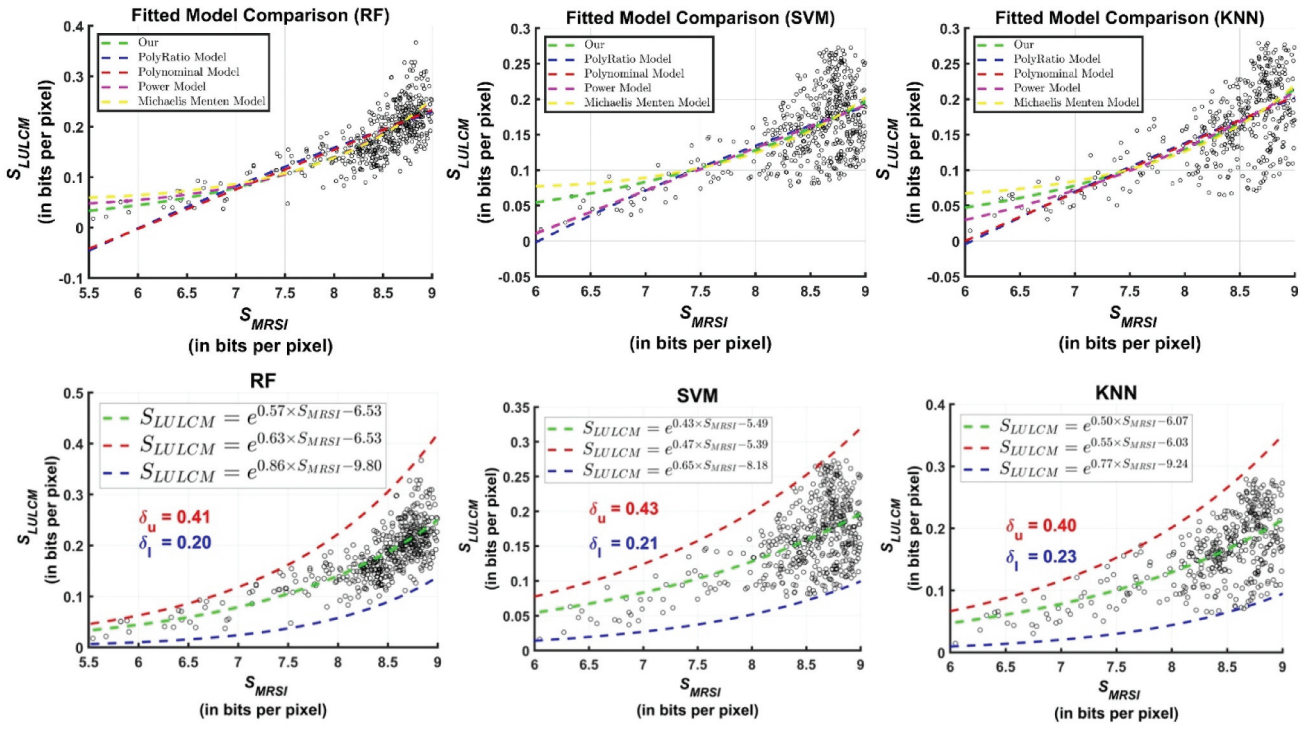

Figure 10. Upper and lower bounds of information transfer from MRSI to LULCM. The top panel shows the fitted models, and the bottom panel demonstrates the best fitted line and corresponding upper and lower bounds. δ_u is the area between the dashed red line and the dashed green line, while δ_l represents the area between the dashed green line and the dashed blue line.

Table 2. Boltzmann-entropy-based upper and lower bounds. GI_v denotes the variation.

Classifier	Fitted model	Upper bound	Lower bound	GI_v	Recommended
RF	$e^{0.57\times S_{MRSI}-6.53}$	$e^{0.63\times S_{MRSI}-6.53}$	$e^{0.86\times S_{MRSI}-9.80}$	2.05	yes
SVM	$e^{0.43\times S_{MRSI}-5.49}$	$e^{0.47\times S_{MRSI}-5.39}$	$e^{0.65\times S_{MRSI}-8.18}$	2.05	no
KNN	$e^{0.50\times S_{MRSI}-6.07}$	$e^{0.55\times S_{MRSI}-6.03}$	$e^{0.77\times S_{MRSI}-9.24}$	1.74	no

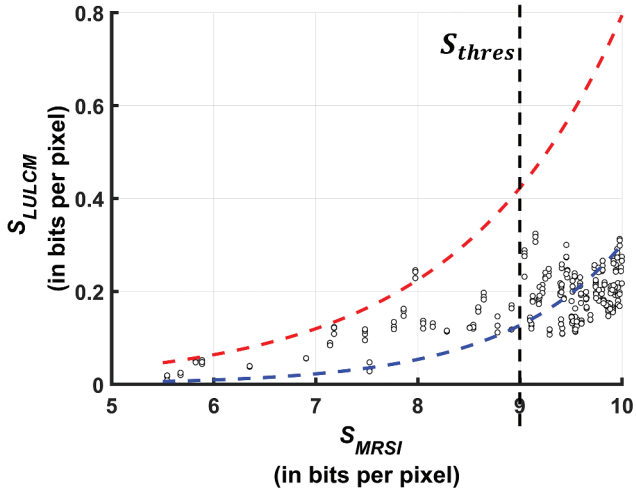

Figure 11. Graphical examination of the recommended model of upper and lower limits.

6. Conclusion

Land cover classification is essential for a variety of applications, from public health to carbon cycle modeling. Although numerous classification techniques exist, the upper and lower bounds of land cover classification accuracy remain largely unexamined. This study addresses this gap by employing Crooks' Fluctuation Theorem alongside Boltzmann entropy to model the information transfer from images to maps. We begin by defining thermodynamic concepts for images, maps, and land cover classification and discussing how these definitions align with those used in thermodynamics. Ultimately, we propose a Boltzmann-entropy-based model incorporating Boltzmann entropies of MRSI and LULCM, the total number of classes in the LULCM, classification accuracy (i.e. weighted F1-score), and two parameters specifically tailored with prior

knowledge. This model achieves high predictive accuracy with minimal parameters.

The computation of S_{MRSI} is efficient, taking less than 1 s for a 500×500 MRSI with six bands on an Intel Core i7–4790 CPU @ 3.60 GHz with 8.00 GB RAM and a 64-bit Windows 10 environment. Consequently, the Boltzmann-entropy-based model can be flexibly applied to optimize land cover classification processes and verify classification accuracy with limited or no ground reference data on large spatial scales. Moreover, our model is adaptable to any patch size of 2×2 or larger, allowing flexibility in assessing agreement between map and reference.

Most importantly, the model establishes an explicit relationship between MRSI and LULCM, providing information-based insights that can inform the design of more robust land cover classification frameworks. It also lays the foundation for developing an information theory tailored to remote sensing image analysis.

Disclosure statement

No potential conflict of interest was reported by the author(s).

Funding

This work was supported by the NSFC (project 41930104), Southwest Jiaotong University and the Research Grants Council of Hong Kong Special Administrative Region (GRF 15221918). We give heartfelt thanks to Prof Bo Wu at the Department of Land Surveying and Geo-Informatics of the Hong Kong Polytechnic University for providing support in labeling images. We use ChatGPT to polish sentences and figure captions.

ORCID

Xinghua Cheng http://orcid.org/0000-0002-1931-6174
Zhilin Li http://orcid.org/0000-0003-1507-323X

CRediT authorship contribution statement

Xinghua Cheng: Conceptualization, Data curation, Formal analysis, Investigation, Methodology, Software, Validation, Visualization, Writing – original draft, Writing – review and editing.

Zhilin Li: Conceptualization, Funding acquisition, Supervision, Writing – original draft, Writing – review and editing.

Data availability statement

For the codes of calculating Boltzmann entropy, interested users may contact Xinghua Cheng at cxh9791156936@gmail.com.

References

Anderson, J. R. 1971. "Land Use Classification Schemes." *Photogrammetric Engineering* 37:379–387. https://trid.trb.org/View/93641.

Baraldi, A., L. Bruzzone, and P. Blonda. 2005. "Quality Assessment of Classification and Cluster Maps without Ground Truth Knowledge." *IEEE Transactions on Geoscience & Remote Sensing* 43 (4): 857–873. https://doi.org/10.1109/TGRS.2004.843074.

Benz, U. C., P. Hofmann, G. Willhauck, I. Lingenfelder, and M. Heynen. 2004. "Multi-Resolution, Object-Oriented Fuzzy Analysis of Remote Sensing Data for GIS-Ready Information." *Isprs Journal of Photogrammetry & Remote Sensing* 58 (3): 239–258. https://doi.org/10.1016/j.isprsjprs.2003.10.002.

Boltzmann, L. 1872. "Weitere studien über das wärmegleichgewicht unter gasmolekülen [Further studies on the thermal equilibrium of gas molecules]." *Aus der kk Hot-und Staatsdruckerei* 66:275–370. https://doi.org/10.1515/9783112596760-011.

Breiman, L. 2001. "Random Forests." *Machine Learning* 45 (1): 5–32. https://doi.org/10.1023/A:1010933404324.

Chen, B., B. Huang, and B. Xu. 2017. "Multi-Source Remotely Sensed Data Fusion for Improving Land Cover Classification." *Isprs Journal of Photogrammetry & Remote Sensing* 124:27–39. https://doi.org/10.1016/j.isprsjprs.2016.12.008.

Chen, Y., Q. Liu, J. Yang, X. Cheng, and M. Deng. 2024. "Spatially Constrained Statistical Approach for Determining the Optimal Number of Regions in Regionalization." *International Journal of Geographical Information Science* 38 (10): 1–40. https://doi.org/10.1080/13658816.2024.2372779.

Cheng, X., and Z. Li. 2021. "Predicting the Lossless Compression Ratio of Remote Sensing Images with Configurational Entropy." *IEEE Journal of Selected Topics in Applied Earth Observations & Remote Sensing* 14:11936–11953. https://doi.org/10.1109/JSTARS.2021.3123650.

Cheng, X., and Z. Li. 2023. "Modeling Information Flow from Multispectral Remote Sensing Images to Land Use and Land Cover Maps for Understanding Classification Mechanism." *Geo-Spatial Information Science* 27 (5): 1568–1584. https://doi.org/10.1080/10095020.2023.2275625.

Cheng, X., and W. Yeung Yan. 2025. "Inferring Radiometric Quality of Multispectral Airborne Laser Scanning Data." *Journal of Geovisualization and Spatial Analysis* 9 (1): 12. https://doi.org/10.1007/s41651-025-00213-8.

Crooks, G. E. 1999. "Entropy Production Fluctuation Theorem and the Nonequilibrium Work Relation for Free Energy Differences." *Physical Review E* 60 (3): 2721–2726. https://doi.org/10.1103/PhysRevE.60.2721.

Cushman, S. A. 2016. "Calculating the Configurational Entropy of a Landscape Mosaic." *Landscape Ecology* 31 (3): 481–489. https://doi.org/10.1007/s10980-015-0305-2.

Denham, R., K. Mengersen, and C. Witte. 2009. "Bayesian Analysis of Thematic Map Accuracy Data." *Remote Sensing of Environment* 113 (2): 371–379. https://doi.org/10.1016/j.rse.2008.10.008.

Ebrahimy, H., B. Mirbagheri, A. Akbar Matkan, and M. Azadbakht. 2021. "Per-Pixel Land Cover Accuracy Prediction: A Random Forest-Based Method with Limited Reference Sample Data." *Isprs Journal of Photogrammetry & Remote Sensing* 172:17–27. https://doi.org/10.1016/j.isprsjprs.2020.11.024.

Fauvel, M., J. Chanussot, and J. Atli Benediktsson. 2006. "Decision Fusion for the Classification of Urban Remote Sensing Images." *IEEE Transactions on Geoscience & Remote Sensing* 44 (10): 2828–2838. https://doi.org/10.1109/TGRS.2006.876708.

Foody, G. M. 2010. "Assessing the Accuracy of Land Cover Change with Imperfect Ground Reference Data." *Remote Sensing of Environment* 114 (10): 2271–2285. https://doi.org/10.1016/j.rse.2010.05.003.

Foody, G. M., and A. Mathur. 2006. "The Use of Small Training Sets Containing Mixed Pixels for Accurate Hard Image Classification: Training on Mixed Spectral Responses for Classification by a SVM." *Remote Sensing of Environment* 103 (2): 179–189. https://doi.org/10.1016/j.rse.2006.04.001.

Franco-Lopez, H., A. R. Ek, and M. E. Bauer. 2001. "Estimation and Mapping of Forest Stand Density, Volume, and Cover Type Using the *K*-Nearest Neighbors Method." *Remote Sensing of Environment* 77 (3): 251–274. https://doi.org/10.1016/S0034-4257(01)00209-7.

Gale, M. G., G. J. Cary, A. I. J. M. Van Dijk, and M. Yebra. 2021. "Forest Fire Fuel Through the Lens of Remote Sensing: Review of Approaches, Challenges and Future Directions in the Remote Sensing of Biotic Determinants of Fire Behaviour." *Remote Sensing of Environment* 255:112282. https://doi.org/10.1016/j.rse.2020.112282.

Gao, P., and Z. Li. 2019. "Computation of the Boltzmann Entropy of a Landscape: A Review and a Generalization." *Landscape Ecology* 34:2183–2196. https://doi.org/10.1007/s10980-019-00814-x.

Gao, P., Z. Li, and H. Zhang. 2018. "Thermodynamics-Based Evaluation of Various Improved Shannon Entropies for Configurational Information of Gray-Level Images." *Entropy* 20 (1): 19. https://doi.org/10.3390/e20010019.

Gao, P., J. Wang, H. Zhang, and Z. Li. 2018. "Boltzmann Entropy-Based Unsupervised Band Selection for Hyperspectral Image Classification." *IEEE Geoscience & Remote Sensing Letters* 16 (3): 462–466. https://doi.org/10.1109/LGRS.2018.2872358.

Gao, P., H. Zhang, and Z. Li. 2017. "A Hierarchy-Based Solution to Calculate the Configurational Entropy of Landscape Gradients." *Landscape Ecology* 32 (6): 1133–1146. https://doi.org/10.1007/s10980-017-0515-x.

Gong, P., J. Wang, and H. Huang. 2024. "Stable Classification with Limited Samples in Global Land Cover Mapping: Theory and Experiments." *Science Bulletin* 69 (12): 1862–1865. https://doi.org/10.1016/j.scib.2024.03.040.

Hartling, S., V. Sagan, and M. Maimaitijiang. 2021. "Urban Tree Species Classification Using UAV-Based Multi-Sensor Data Fusion and Machine Learning." *GIScience & Remote Sensing* 58 (8): 1250–1275. https://doi.org/10.1080/15481603.2021.1974275.

Heydari, S. S., and G. Mountrakis. 2018. "Effect of Classifier Selection, Reference Sample Size, Reference Class Distribution and Scene Heterogeneity in Per-Pixel Classification Accuracy Using 26 Landsat Sites." *Remote Sensing of Environment* 204:648–658. https://doi.org/10.1016/j.rse.2017.09.035.

Hong, D., B. Zhang, H. Li, L. Yuxuan, J. Yao, C. Li, M. Werner, J. Chanussot, A. Zipf, and X. Xiang Zhu. 2023. "Cross-City Matters: A Multimodal Remote Sensing Benchmark Dataset for Cross-City Semantic Segmentation Using High-Resolution Domain Adaptation Networks." *Remote Sensing of Environment* 299:113856. https://doi.org/10.1016/j.rse.2023.113856.

Khatami, R., G. Mountrakis, and S. V. Stehman. 2017. "Mapping Per-Pixel Predicted Accuracy of Classified Remote Sensing Images." *Remote Sensing of Environment* 191:156–167. https://doi.org/10.1016/j.rse.2017.01.025.

Li, Y., Y. Zhou, Y. Zhang, L. Zhong, J. Wang, and J. Chen. 2022. "DKDFN: Domain Knowledge-Guided Deep Collaborative Fusion Network for Multimodal Unitemporal Remote Sensing Land Cover Classification." *Isprs Journal of Photogrammetry & Remote Sensing* 186:170–189. https://doi.org/10.1016/j.isprsjprs.2022.02.013.

Lin, D., K. Fu, Y. Wang, G. Xu, and X. Sun. 2017. "MARTA GANs: Unsupervised Representation Learning for Remote Sensing Image Classification." *IEEE Geoscience & Remote Sensing Letters* 14 (11): 2092–2096. https://doi.org/10.1109/LGRS.2017.2752750.

Lu, D., and Q. Weng. 2007. "A Survey of Image Classification Methods and Techniques for Improving Classification Performance." *International Journal of Remote Sensing* 28 (5): 823–870. https://doi.org/10.1080/01431160600746456.

Ma, A., C. Zheng, J. Wang, and Y. Zhong. 2023. "Domain Adaptive Land-Cover Classification via Local Consistency and Global Diversity." *IEEE Transactions on Geoscience & Remote Sensing* 61:1–17. https://doi.org/10.1109/TGRS.2023.3265186.

Magnussen, S. 2009. "A Bayesian Approach to Classification Accuracy Inference." *Forestry: An International Journal of Forest Research* 82 (2): 211–226. https://doi.org/10.1093/forestry/cpp001.

Mahdavi, S., B. Salehi, J. Granger, M. Amani, B. Brisco, and W. Huang. 2018. "Remote Sensing for Wetland Classification: A Comprehensive Review." *GIScience & Remote Sensing* 55 (5): 623–658. https://doi.org/10.1080/15481603.2017.1419602.

Olofsson, P., G. M. Foody, M. Herold, S. V. Stehman, C. E. Woodcock, and M. A. Wulder. 2014. "Good Practices for Estimating Area and Assessing Accuracy of Land

Change." *Remote Sensing of Environment* 148:42–57. https://doi.org/10.1016/j.rse.2014.02.015.

Pedregosa, F., G. Varoquaux, A. Gramfort, Michel, V, Thirion, B, Grisel, O, Blondel, M, Prettenhofer, P, Weiss, R, Dubourg, V, Vanderplas, J. 2011. "Scikit-Learn: Machine Learning in Python." *Journal of Machine Learning Research* 12:2825–2830. https://doi.org/10.5555/1953048.2078195.

Romero, A., C. Gatta, and G. Camps-Valls. 2016. "Unsupervised Deep Feature Extraction for Remote Sensing Image Classification." *IEEE Transactions on Geoscience & Remote Sensing* 54 (3): 1349–1362. https://doi.org/10.1109/TGRS.2015.2478379.

Shannon, C. E. 1948. "A Mathematical Theory of Communication." *Bell System Technical Journal* 27 (3): 379–423. https://doi.org/10.1002/j.1538-7305.1948.tb01338.x.

Sheng, Y., C. Song, J. Wang, E. A. Lyons, B. R. Knox, J. S. Cox, and F. Gao. 2016. "Representative Lake Water Extent Mapping at Continental Scales Using Multi-Temporal Landsat-8 Imagery." *Remote Sensing of Environment* 185:129–141. https://doi.org/10.1016/j.rse.2015.12.041.

Stehman, S. V. 2009a. "Sampling Designs for Accuracy Assessment of Land Cover." *International Journal of Remote Sensing* 30 (20): 5243–5272. https://doi.org/10.1080/01431160903131000.

Stehman, S. V. 2009b. "Model-Assisted Estimation as a Unifying Framework for Estimating the Area of Land Cover and Land-Cover Change from Remote Sensing." *Remote Sensing of Environment* 113 (11): 2455–2462. https://doi.org/10.1016/j.rse.2009.07.006.

Stehman, S. V., and G. M. Foody. 2019. "Key Issues in Rigorous Accuracy Assessment of Land Cover Products." *Remote Sensing of Environment* 231:111199. https://doi.org/10.1016/j.rse.2019.05.018.

Stehman, S. V., J. Mousoupetros, R. E. McRoberts, E. Næsset, B. W. Pengra, D. Xing, and J. A. Horton. 2022. "Incorporating Interpreter Variability into Estimation of the Total Variance of Land Cover Area Estimates Under Simple Random Sampling." *Remote Sensing of Environment* 269:112806. https://doi.org/10.1016/j.rse.2021.112806.

Stehman, S. V., and J. D. Wickham. 2011. "Pixels, Blocks of Pixels, and Polygons: Choosing a Spatial Unit for Thematic Accuracy Assessment." *Remote Sensing of Environment* 115 (12): 3044–3055. https://doi.org/10.1016/j.rse.2011.06.007.

Tong, X.-Y., G.-S. Xia, Q. Lu, H. Shen, S. Li, S. You, and L. Zhang. 2020. "Land-Cover Classification with High-Resolution Remote Sensing Images Using Transferable Deep Models." *Remote Sensing of Environment* 237:111322. https://doi.org/10.1016/j.rse.2019.111322.

Weiss, M., F. Jacob, and G. Duveiller. 2020. "Remote Sensing for Agricultural Applications: A Meta-Review." *Remote Sensing of Environment* 236:111402. https://doi.org/10.1016/j.rse.2019.111402.

Wickham, J., S. V. Stehman, D. G. Sorenson, L. Gass, and J. A. Dewitz. 2021. "Thematic Accuracy Assessment of the NLCD 2016 Land Cover for the Conterminous United States." *Remote Sensing of Environment* 257:112357. https://doi.org/10.1016/j.rse.2021.112357.

Wickham, J., S. V. Stehman, D. G. Sorenson, L. Gass, and J. A. Dewitz. 2023. "Thematic Accuracy Assessment of the NLCD 2019 Land Cover for the Conterminous United States." *GIScience & Remote Sensing* 60 (1): 2181143. https://doi.org/10.1080/15481603.2023.2181143.

Wulder, M. A., S. E. Franklin, J. C. White, J. Linke, and S. Magnussen. 2006. "An Accuracy Assessment Framework for Large-Area Land Cover Classification Products Derived from Medium-Resolution Satellite Data." *International Journal of Remote Sensing* 27 (4): 663–683. https://doi.org/10.1080/01431160500185284.

Xing, D., and S. V. Stehman. 2024. "Using Interpenetrating Subsampling to Incorporate Interpreter Variability into Estimation of the Total Variance of Land Cover Area Estimates." *Remote Sensing of Environment* 311:114289. https://doi.org/10.1016/j.rse.2024.114289.

Yu, X., X. Wu, C. Luo, and P. Ren. 2017. "Deep Learning in Remote Sensing Scene Classification: A Data Augmentation Enhanced Convolutional Neural Network Framework." *GIScience & Remote Sensing* 54 (5): 741–758. https://doi.org/10.1080/15481603.2017.1323377.

Yuan, Q., H. Shen, T. Li, L. Zhiwei, L. Shuwen, Y. Jiang, H. Xu, et al. 2020. "Deep Learning in Environmental Remote Sensing: Achievements and Challenges." *Remote Sensing of Environment* 241:111716. https://doi.org/10.1016/j.rse.2020.111716.

Zhu, Q., Y. Lei, X. Sun, Q. Guan, Y. Zhong, L. Zhang, and D. Li. 2022. "Knowledge-Guided Land Pattern Depiction for Urban Land Use Mapping: A Case Study of Chinese Cities." *Remote Sensing of Environment* 272:112916. https://doi.org/10.1016/j.rse.2022.112916.

Zhu, Z., and C. E. Woodcock. 2014. "Continuous Change Detection and Classification of Land Cover Using All Available Landsat Data." *Remote Sensing of Environment* 144:152–171. https://doi.org/10.1016/j.rse.2014.01.011.